Scripta Materialia 142 (2018) 111–115

Contents lists available at ScienceDirect

Scripta Materialia

journal homepage: www.elsevier.com/locate/scriptamat

Regular article

Plastic deformation mechanisms of biomedical Co–Cr–Mo alloy single crystals with hexagonal close-packed structure

Wataru Kaita [a], Koji Hagihara [b], Luís Augusto Rocha [c,d,e], Takayoshi Nakano [a,*]

[a] Division of Materials Science and Engineering, Graduate School of Engineering, Osaka University, 2-1 Yamadaoka, Suita, Osaka 565-0871, Japan
[b] Department of Adaptive Machine Systems, Graduate School of Engineering, Osaka University, 2-1 Yamadaoka, Suita, Osaka 565-0871, Japan
[c] Center of MicroElectroMechanical Systems, Department of Mechanical Engineering, University of Minho, Campus de Azurém, Guimarães 4800-058, Portugal
[d] IBTN/Br–Brazilian Branch of the Institute of Biomaterials, Tribocorrosion and Nanomedicine, Universidade Estadual Paulista–UNESP, Av. Eng. Luiz Edmundo Carrijo Coube, Bauru 17033-360, São Paulo, Brazil
[e] Faculdade de Ciências, Departamento de Física, Universidade Estadual Paulista–UNESP, Av. Eng. Luiz Edmundo Carrijo Coube, Bauru 17033-360, São Paulo, Brazil

ARTICLE INFO

Article history:
Received 16 June 2017
Received in revised form 8 August 2017
Accepted 10 August 2017
Available online 29 August 2017

Keywords:
Biomaterials
Co–Cr–Mo alloy
Single crystal
Deformation mode
Dislocation

ABSTRACT

This is the first report of the successful fabrication of Co–Cr–Mo biomedical alloy single crystals with a hexagonal close-packed (hcp) structure and the resultant clarification of its deformation behavior. The (0001) $\langle 11\bar{2}0\rangle$ basal and $\{1\bar{1}00\}$ $\langle 11\bar{2}0\rangle$ prismatic slip systems were found to be predominately operative. The critical resolved shear stresses for the basal and prismatic slip systems at ambient temperature are ~204 and ~272 MPa, respectively, which are much higher than ~54 MPa for $\{111\}$ $\langle 11\bar{2}\rangle$ slip in the face-centered cubic (fcc) Co–Cr–Mo phase, quantitatively demonstrating that the hcp phase acts as an effective strengthening phase.

Co–Cr–Mo alloys have been widely applied for surgical implants such as the hip joint (femoral head) and artificial knee joint owing to their high strength, high corrosion resistance, superior wear behavior, and modest biocompatibility [1–3]. Generally, Co–Cr–Mo alloys predominately consist of an fcc phase, the γ-phase [2]. Thermodynamically, however, the γ-phase is stable only at high temperatures and transforms into the hcp structure, the ε-phase, by a heat treatment at low temperatures [4]. Many studies of the mechanical properties of Co–Cr–Mo alloys have been conducted using polycrystals [5–11]. However, the deformation behavior of Co–Cr–Mo alloys is complex because it is affected by numerous parameters including the grain size, texture, heat-treatment conditions, etc. in the polycrystalline form. Thus, the study of single crystals is strongly required to understand the mechanisms that control the deformation behavior from a fundamental viewpoint. In addition, we have recently proposed the development of "single-crystal implant materials" in β-Ti alloys [12,13], which allows the superior characteristics of metallic biomaterials to be fully attained by controlling the crystal orientation. It is strongly expected that a similar strategy must be applicable to Co–Cr–Mo alloys. Thus, the study of single crystals is essential to further development of Co–Cr–Mo alloys for biomedical implant applications.

With this background, we recently conducted a study with a γ(fcc)-phase single crystal and clarified the strong orientation and microstructural dependence of the plastic deformation behavior [14]. As a predominant deformation mechanism at room temperature (RT), a strain-induced martensitic transformation (SIM) from the γ-phase to the ε-phase was confirmed.

On the other hand, even though the ε-phase is considered to be the essential phase for improving the wear resistance [15] and increasing the strength of Co–Cr–Mo alloys [14,16,17], its deformation mechanism has not yet been sufficiently clarified. This has been a major obstacle for the development of novel artificial joints with superior mechanical properties, and is derived from the difficulties associated with the fabrication of ε-phase single crystals. This is because the transformation to the ε-phase from the γ-phase must accompany the formation of four variant grains with different crystal orientations, as detailed later. Overcoming this obstacle, the new strategy for fabrication of an ε-phase single crystal is reported for the first time in this paper, and the deformation mechanism is clarified.

In the experimental procedure, a mother ingot with a composition of Co–27Cr–6Mo (in wt%), as defined by ASTM F75, was supplied by Teijin Nakashima Medical Co. Ltd., Japan. Using the mother ingot, a single crystal was grown by the Bridgman method at a growth rate of 5 mm/h in an Ar atmosphere in an Al_2O_3 crucible. By X-ray Laue back diffraction, the obtained single crystal was confirmed to predominantly consist of the γ-phase with the fcc structure [14]. Then, a heat treatment was

* Corresponding author.
E-mail address: nakano@mat.eng.osaka-u.ac.jp (T. Nakano).

http://dx.doi.org/10.1016/j.scriptamat.2017.08.016

conducted for 15 and 40 h at 800 °C to obtain an ε-phase single crystal with the hcp structure. In some specimens, compressive deformation was applied at RT prior to the heat treatment to enhance the phase transformation from the γ-phase to the ε-phase. The predeformation was conducted by using the specimen with dimensions of ~2.0 × 5.0 × 5.0 mm^3 and a $[\bar{1}49]_{fcc}$ loading orientation. The variation in the microstructure was examined by transmission electron microscopy (TEM; JEOL JEM-3010) and electron backscatter diffraction pattern analysis during scanning electron microscopy (SEM-EBSD; JEOL JSM-6500F).

By using the ε-phase single crystal, the plastic deformation behavior was examined by a compression test. Rectangular specimens with dimensions of ~1.6 × 1.6 × 4.0 mm^3 were cut by electrodischarge machining. Two loading orientations parallel to $[1\ 1\ \bar{2}\ 1.86]_{hcp}$ and $[1\ 1\ \bar{2}\ 0]_{hcp}$ were chosen to clarify the orientation dependence of the deformation behavior. The Schmid factors for the possible deformation modes in the ε-phase are listed in Supplementary Table 1. Compression tests were conducted at RT at a nominal strain rate of 1.67×10^{-4} s^{-1} in vacuum. Deformation markings introduced in the specimens were observed by an optical microscope equipped with Normarski interference contrast, and the further details of the deformation substructures were examined by TEM.

Fig. 1(a–i) show the crystal orientation maps for the ε-phase acquired by SEM-EBSD, showing the variation in the volume fraction of the ε-phase and microstructure due to predeformation and the subsequent heat treatment of the Co–Cr–Mo alloy single crystals. As reported previously [14], the single crystal obtained by the Bridgman method predominantly consists of the γ-phase (shown in black in Fig. 1), but small amounts of the ε(hcp)-phase are also present with a stacking-fault-like morphology, as shown in Fig. 1(a). It is well-known that the ε-phase frequently forms with the following Shoji–Nishiyama relationship in the γ-matrix-phase [18]:

$$\{111\}_\gamma \,//\, (0001)_\varepsilon,\ \langle 11\bar{2}\rangle_\gamma \,//\, \langle 01\bar{1}0\rangle_\varepsilon,\ \langle 1\bar{1}0\rangle_\gamma \,//\, \langle 2\bar{1}\bar{1}0\rangle_\varepsilon \quad (1)$$

Thus, the ε-phase formed by the conventional heat treatment generally exhibits four variants with a habit plane parallel to (111), $(\bar{1}11)$, $(1\bar{1}1)$, or $(11\bar{1})$. However, in the Co–Cr–Mo single crystal grown by our Bridgman method, only one of the four ε-variants with the habit plane of (111) was predominantly present, probably because of strain relaxation during the γ-to-ε phase transformation [14]. After the annealing of the as-grown single crystal, however, the abovementioned four variants were almost equivalently formed, as shown in Fig. 1(d, g). Thus, the ε-single-phase single crystal cannot be obtained by the simple annealing of the γ-phase single crystal. To overcome this problem, a small prestrain was imparted to the crystal prior to the heat treatment. The prestrain was imparted by compression deformation in the $[\bar{1}49]$ orientation at RT, by which the SIM whose habit plane is parallel to (111), i.e., the same as that of the grown-in ε-variant, could be selectively formed by the operation of $a/6\ \langle\bar{1}\bar{1}2\rangle$ Shockley partial dislocations [14]. Actually, the volume fraction of the ε-phase increased as the applied prestrain increased, and for the specimen with 5% plastic strain, the γ-phase was regarded to be almost fully transformed into the ε-phase via evaluation by SEM-EBSD (Fig. 1(c)). The features developed in the microstructure by annealing also strongly varied with the amount of applied prestrain. By applying a prestrain of 1% to the specimen, the volume fraction of the ε-phase reached almost 100% after subsequent annealing for 15 h (Fig. 1(e)); nevertheless, it was still ~59% in the nondeformed specimen (Fig. 1(d)). However, some variants formed by the heat treatment did not match the grown-in variant; hence, a single-variant single crystal could not be obtained by annealing the 1%-deformed specimen. On the other hand, for the specimen with 5% prestrain, the specimen was almost fully covered by ε-phase just by deformation (Fig. 1(c)), and almost no change in the crystal orientation occurred after subsequent annealing for 15 h (Fig. 1(f)), although the formation of some low-angle boundaries was observed. However, when the annealing time was extended to 40 h for the 5%-deformed specimen, many ε-phase grains developed with a different crystal orientation than the abovementioned variant orientation relationship. These grains are considered to be recrystallized grains; thus, the single-crystal microstructure collapsed owing to their development, as shown in Fig. 1(i).

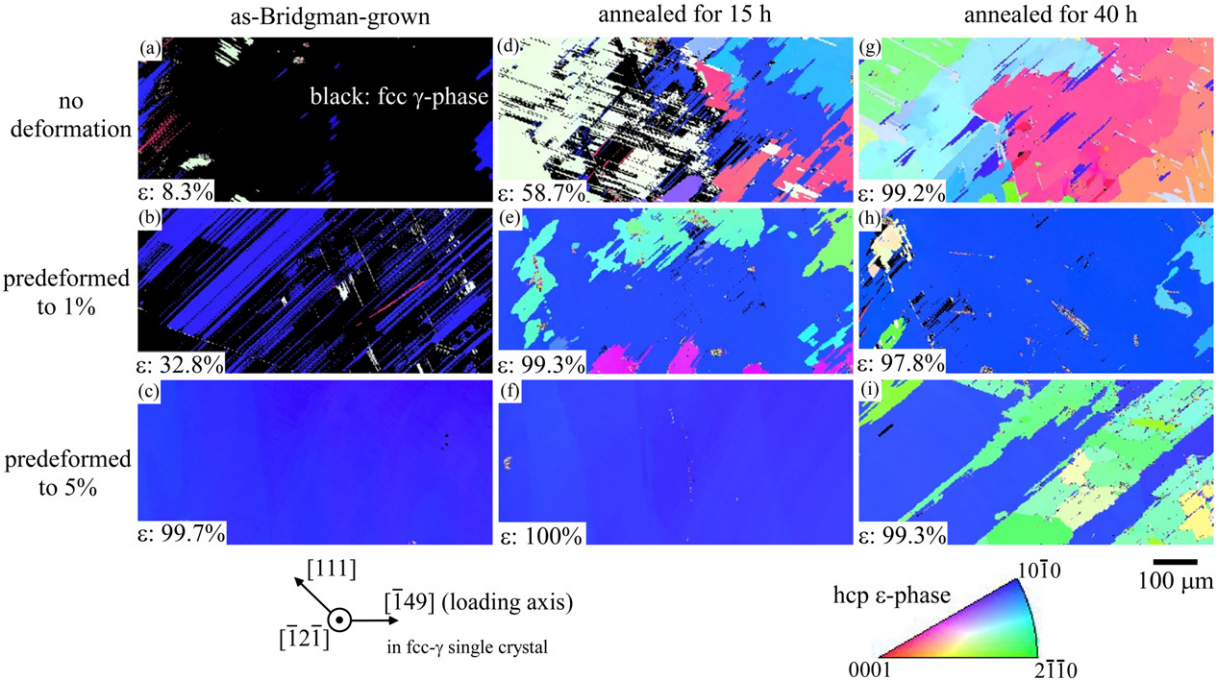

Fig. 1. (a–i) Crystal orientation maps for the hcp ε-phase, showing the variation in its volume fraction and microstructure in a Co–Cr–Mo fcc γ-phase single crystal for various levels of predeformation and subsequent heat treatments. The black regions correspond to the γ-phase.

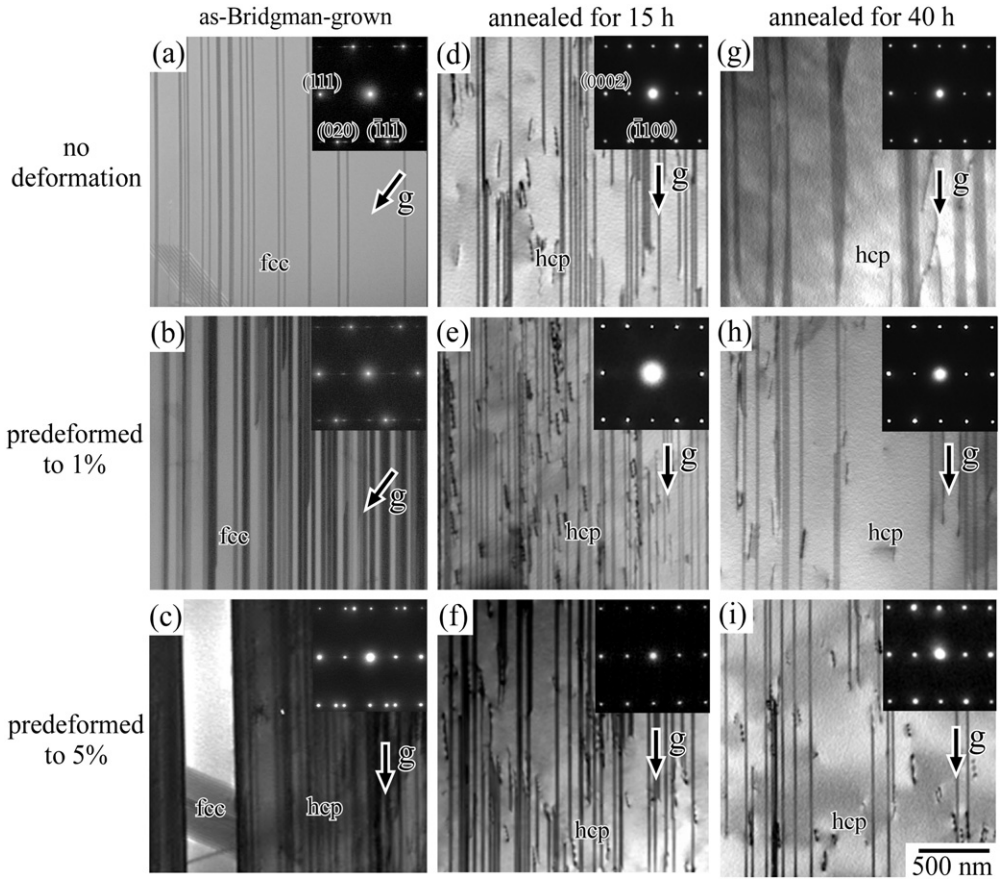

Fig. 2. (a–i) TEM bright-field images showing the variation in the microstructure of a Co–Cr–Mo single crystal for various levels of predeformation and subsequent heat treatments. Beam // $[10\bar{1}]$, diffraction vector (**g**) = $(020)_\gamma$ in Panels (a, b) and = $(\bar{2}200)_\varepsilon$ in Panels (c–i).

Fig. 2(a–i) show the bright-field TEM images acquired for the specimens in Fig. 1. The corresponding electron diffraction patterns (DPs) are shown in the insets of the figures. As described above, small amounts of the ε-phase exist with a stacking-fault-like morphology in the as-grown crystal, and the volume fraction of the ε-phase increased as the applied prestrain increased (Fig. 2(a–c)). However, it was confirmed that some amounts of the γ-phase still remained even in the 5% prestrained specimen, in contrast to the results from the SEM-EBSD analysis. This is due to the difficulties associated with the detection of the thin γ-phases in the ε-phase during SEM-EBSD due to the limited resolution and the similarity of the fcc and hcp crystal structures having the same close-packed planes, similar to previous results obtained for lamellar TiAl alloys [19]. In the annealed specimens with the prestrain, however, such thin γ-phases in the ε-phase grains almost disappeared, although some stacking

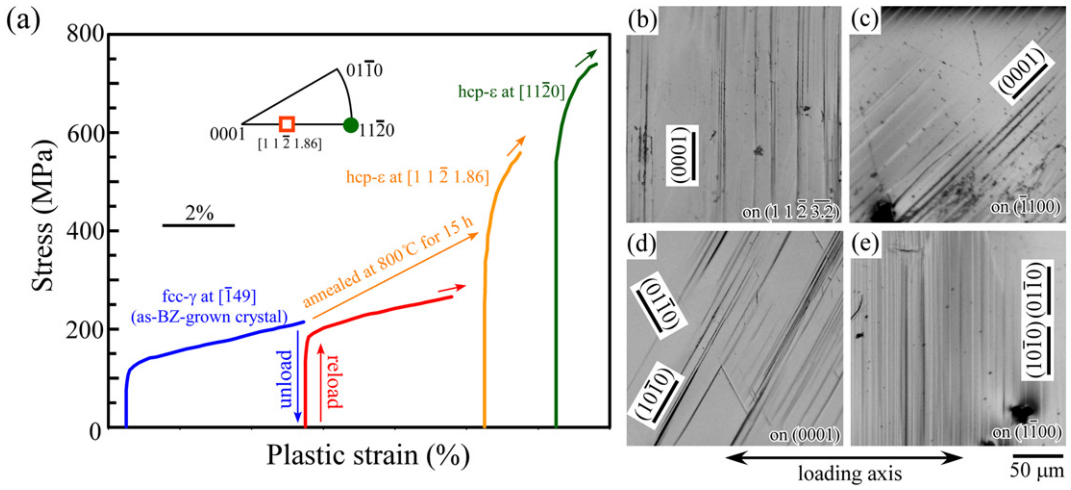

Fig. 3. (a) Variations in the stress–strain curves of Co–Cr–Mo single crystals with heat treatment and loading orientation obtained by compression tests at RT. (b–e) Slip traces observed in the ε-single-phase single crystals deformed in the (b, c) [1 1 $\bar{2}$ 1.86] and (d, e) [11$\bar{2}$0] loading orientations.

faults remained in the grains (Fig. 2(d–i)). From these results, it is concluded that an ε-phase single crystal can be obtained by annealing the specimen at 800 °C for 15 h, which was previously predeformed in the [$\bar{1}$49] orientation to 5% plastic strain at RT. Using this "ε-phase single crystal," the plastic deformation behavior of the ε-phase was examined.

Fig. 3(a) shows the typical stress–strain curves of the ε-phase single crystal deformed in the [1 1 $\bar{2}$ 1.86] and [11$\bar{2}$0] orientations. In this graph, the stress–strain curve of the γ-phase single crystal deformed in the [$\bar{1}$49] orientation, i.e., the stress–strain curve for the sample subjected to the predeformation treatment, is also plotted for comparison. Note that the [1 1$\bar{2}$1.86] loading orientation in the ε-phase single crystal is exactly parallel to the [$\bar{1}$49] loading orientation in the γ-phase single crystal selected in the predeformation. When the γ-phase single crystal was compressed to 5% plastic strain (blue curve) and then reloaded, the specimen reyielded at a stress of ~191 MPa (red curve). This value was close to the flow stress at the 5% strain in the previous test, as a matter of course. However, by annealing the 5%-predeformed specimen, the yield stress became as high as ~408 MPa on average (yellow curve). This obviously demonstrates that the phase transformation from the γ-phase to the ε-phase increases the yield stress. The yield stress also varied according to the loading orientation, and the average yield stress of the ε-phase single crystal in the [11$\bar{2}$0] orientation was higher at ~627 MPa (green curve). The variations in stress-strain curves in largely deformed region after yielding have not been sufficiently examined yet, owing to the limitation of the number of obtained single-crystalline specimen.

Fig. 3(b–e) show the slip traces observed in the 1%-deformed "ε-phase single crystal" specimens. The operation of different slip systems depending on the loading axis was confirmed. A two-face trace analysis demonstrated that (0001) basal slip and {10$\bar{1}$0} prismatic slip were operative in the [1 1 $\bar{2}$ 1.86] and [11$\bar{2}$0] orientations, respectively. The Burgers vectors of the dislocations for these slip systems were examined by TEM. Fig. 4(a, b) show bright-field images of dislocations for the specimen deformed in the [11$\bar{2}$0] orientation observed on the (10$\bar{1}$0) slip plane. Many dislocations were visible with a diffraction vector $\mathbf{g} = (1\bar{2}10)$. The dislocations showed straight morphologies aligned along the [1$\bar{2}$10] direction (Fig. 4(a)). However, these dislocations lost their contrast when observed with $\mathbf{g} = (0002)$ (Fig. 4(b)). Taking their (10$\bar{1}$0) slip plane into consideration, the observation results suggest that (10$\bar{1}$0)[1$\bar{2}$10] slip was operative. A dislocation analysis was also conducted for the specimen in which basal slip occurred. The Burgers vector of the predominately operative dislocations on the basal plane was also parallel to ⟨11$\bar{2}$0⟩, as shown in Figs. 4(c, d). Many dislocations exhibited straight morphologies with a screw character. In addition, a ⟨10$\bar{1}$0⟩ dislocation as a secondary slip system accompanied by a stacking fault was partly observed, as shown in the lower-right corner of Fig. 4(d). As shown in Fig. 4(a, c), screw dislocations were predominately observed in both of basal and prismatic slips, but more study is required to conclude that their motions govern the deformation behavior of ε-phase, since the present TEM observation is post-mortem.

From these experimental results, the predominately operative deformation modes in the Co–Cr–Mo biomedical alloy single crystals with an hcp structure were clarified to be (0001) ⟨11$\bar{2}$0⟩ basal slip and {1$\bar{1}$00} ⟨11$\bar{2}$0⟩ prismatic slip. In other hcp-structured metals such as Ti and Mg, the operation of other deformation modes, e.g., {11$\bar{2}$2} pyramidal slip, {10$\bar{1}$2} deformation twin, etc. was also reported [20,21]. However, no clear trace for such deformation modes was observed in the central part of the specimen in the present study. This suggests that the critical resolved shear stresses (CRSSs) of those deformation modes are considerably high. As listed in the Supplementary Table 1, when thinking the compression at [0001] loading orientation, not only the basal and prism slips, but also the formation of {10$\bar{1}$2} twin is difficult. The deformation behavior along the c-axis is open question in the present state.

Focusing on the yield stress in the [1 1 $\bar{2}$ 1.86] and [11$\bar{2}$0] orientations, the CRSSs for (0001)⟨11$\bar{2}$0⟩ basal slip and {1$\bar{1}$00}⟨11$\bar{2}$0⟩ prismatic slip were precisely determined to be approximately 204 and 272 MPa, respectively, at RT for the first time. It is noted that the evaluated values were both more than three times higher than that for {111} ⟨11$\bar{2}$⟩ slip in the γ(fcc) phase of ~54 MPa. This evidences that the ε(hcp) phase acts as an effective strengthening phase in the Co–Cr–Mo alloy. In addition, the results demonstrate that the ε-phase shows a strong plastic anisotropy due to the limited operative slip systems, i.e., predominately basal and prismatic slip. The control of this anisotropic mechanical property must be important for developing "single-crystal Co–Cr–Mo alloy implants."

The CRSS for basal slip was found to be lower than that for prismatic slip. This must be related to the lattice constant ratio c/a in the ε-phase, as was partly pointed out in [16,17]. Jones et al. summarized studies of the deformation behavior of hcp-structured pure metals [21]. They suggested that prismatic slip is predominantly operative in metals with a low c/a ratio but a transition of the operative slip system to basal slip occurs as the c/a ratio increases at around 1.59–1.62. Regarding the origin of this transition of the predominate slip system, Vitek and Igarashi proposed in their computer simulation that the dissociation scheme for a ⟨11$\bar{2}$0⟩ dislocation on the prismatic plane varies with the c/a ratio; dissociation on the prismatic plane is preferred as c/a ratio decreases [22]. Here, the c/a ratio for a Co–Cr–Mo alloy with a similar composition in the ε-phase was previously reported to be ~1.613 [23], which is close to the upper boundary of the c/a ratio where the transition of the slip systems occurs [21]. This must be one of the reasons why both basal and prismatic slips can be operative, but the CRSS for basal slip was lower than that for prismatic slip in the ε-phase.

Matsumoto et al. previously speculated the CRSSs for these slip systems in their study using a polycrystalline alloy [17]. The large difference measured in this study from their speculation is the ratio of the

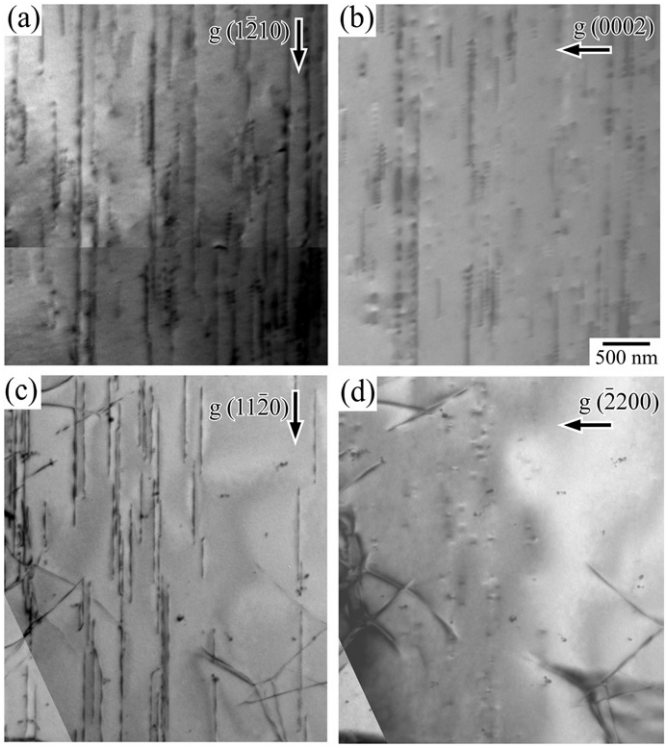

Fig. 4. Bright-field TEM images for an ε-phase single crystal deformed in the (a, b) [11$\bar{2}$0] and (c, d) [1 1 $\bar{2}$ 1.86] loading orientation to ~1% plastic strain. (a, b) Beam // [$\bar{1}$010], $\mathbf{g} = (1\bar{2}10)$ (a), and $\mathbf{g} = (0002)$ (b). (c, d) Beam // [0001], $\mathbf{g} = (11\bar{2}0)$ (c), and $\mathbf{g} = (\bar{2}200)$ (d).

CRSSs for prismatic slip and basal slip. The CRSS ratio for prismatic slip/basal slip is 1.33 in the present study compared to 1.15 for Matsumoto et al. This difference must be derived from the stress concentration effect at the grain boundaries (grain-boundary compatibility stress) in polycrystalline alloys, as the related discussion was reported by Koike et al. for hcp Mg alloys [24].

As another possibility to bring about the difference in CRSS, the influence of the stacking faults against the dislocation motion is supposed. As shown in Fig. 2, in the ε-phase fabricated in the present method, some stacking faults were remained. Koizumi et al. reported the possibility of the occurrence of chemical segregation at the stacking faults by Suzuki effect in Co-Ni alloy [25]. Thus, the stacking faults may act as the effective obstacle for the dislocation motion. The control of the amount of stacking fault and clarification of the influence to the deformation behavior are the issue to be addressed in the future.

The results obtained in this study clarified the importance of the consideration of the strong plastic anisotropy in the ε-phase for understanding the details of the deformation behavior of Co–Cr–Mo alloys, which enables the design of the novel artificial joints with superior mechanical properties.

Supplementary data to this article can be found online at http://dx.doi.org/10.1016/j.scriptamat.2017.08.016.

Acknowledgments

This work was supported by Grants-in-Aid for Scientific Research (S) from the Japan Society for Promotion of Science (Grant No. 25220912).

References

[1] A. Buford, T. Goswami, Mater. Des. 25 (2004) 385–393.
[2] A. Chiba, K. Kumagai, N. Nomura, S. Miyakawa, Acta Mater. 55 (2007) 1309–1318.
[3] Y. Liao, R. Pourzal, P. Stemmer, M.A. Wimmer, J.J. Jacobs, A. Fischer, L.D. Marks, J. Mech. Behav. Biomed. 12 (2012) 39–49.
[4] K.P. Gupta, J. Phase Equilib. Diffus. 26 (2005) 87–92.
[5] A.J. Dempsey, R.M. Pilliar, G.C. Weatherly, T. Kilner, J. Mater. Sci. 22 (1987) 575–581.
[6] A. Salinas-Rodriguez, J.L. Rodriguez-Galicia, J. Biomed. Mater. Res. 31 (1996) 409–419.
[7] P. Huang, H.F. Lopez, Mater. Lett. 39 (1999) 244–248.
[8] K. Yamanaka, M. Mori, S. Kurosu, H. Matsumoto, A. Chiba, Metall. Mater. Trans. A 40A (2009) 1980–1994.
[9] M. Mori, K. Yamanaka, H. Matsumoto, A. Chiba, Mater. Sci. Eng. A 528 (2010) 614–621.
[10] A. Mani, Salinas-Rodriguez, H.F. Lopez, Mater. Sci. Eng. A 528 (2011) 3037–3043.
[11] Y. Koizumi, S. Suzuki, K. Yamanaka, B.-S. Lee, K. Sato, Y. Li, S. Kurosu, H. Matsumoto, A. Chiba, Acta Mater. 61 (2013) 1648–1661.
[12] S.-H. Lee, K. Hagihara, T. Nakano, Metall. Mater. Trans. A 43 (2012) 1588–1597.
[13] K. Hagihara, T. Nakano, H. Maki, Y. Umakoshi, M. Niinomi, Sci. Report. 6 (2016) 29779.
[14] K. Hagihara, T. Nakano, K. Sasaki, Scr. Mater. 123 (2016) 149–153.
[15] A.J. Saldívar-García, H.F. López, J. Biomed, Mater. Res. A 74 (2005) 269–274.
[16] H. Matsumoto, S. Kurosu, B.-S. Lee, Y. Li, A. Chiba, Scr. Mater. 63 (2010) 1092–1095.
[17] H. Matsumoto, Y. Koizumi, T. Ohashi, B.-S. Lee, Y. Li, A. Chiba, Acta Mater. 64 (2014) 1–11.
[18] Z. Nishyama, Martensitic Transformation, Academic Press, Inc., New York, 1978 49.
[19] S. Sitzman, N.-H. Schmidt, A. Palomares-García, R. Muñoz-Moreno, J. Goulden, Microsc. Microanal. 21 (2015) 2037–2038.
[20] M.H. Yoo, Metall. Mater. Trans. A 12 (1981) 409–418.
[21] I.P. Jones, W.B. Hutchinson, Acta Metall. 29 (1981) 951–968.
[22] V. Vitek, M. Igarashi, Philo. Mag. A 63 (1991) 1059–1075.
[23] A.J. Saldívar-García, H.F. López, Metall. Mater. Trans. A 35A (2004) 2517–2523.
[24] J. Koike, T. Kobayashi, T. Mukai, H. Watanabe, M. Suzuki, K. Maruyama, K. Higashi, Acta Mater. 51 (2003) 2055–2065.
[25] Y. Koizumi, T. Nukaya, S. Suzuki, S. Kurosu, Y. Li, H. Matsumoto, K. Sato, Y. Tanaka, A. Chiba, Acta Mater. 60 (2012) 2901–2915.